Electron Diffraction Imaging of Carbon Monoxide via *K*-Shell Ionization by Compton Scattering of 20 keV Photons

D. M. Haubenreißer,[1] N. M. Novikovskiy,[1] N. Melzer,[2] M. Kircher,[2] A. Pier,[2] L. Kaiser,[2] J. Kruse,[2] N. Anders,[2] J. Stindl,[2] L. Sommerlad,[2] O. D. McGinnis,[2] M. Schmidt,[2] L. Nowak,[2] A. Kügler,[2] I. Dwojak,[2] J. Drnec,[3] F. Trinter,[4] M. S. Schöffler,[2] L. Ph. H. Schmidt,[2] T. Jahnke,[5,6] R. Dörner,[2,*] and Ph. V. Demekhin[1,†]

[1]*Institut für Physik und CINSaT, Universität Kassel, Heinrich-Plett-Straße 40, 34132 Kassel, Germany*
[2]*Institut für Kernphysik, Goethe-Universität Frankfurt, Max-von-Laue-Straße 1, 60438 Frankfurt am Main, Germany*
[3]*ESRF, The European Synchrotron, 71 Avenue des Martyrs, CS 40220, 38043 Grenoble Cedex 9, France*
[4]*Molecular Physics, Fritz-Haber-Institut der Max-Planck-Gesellschaft, Faradayweg 4-6, 14195 Berlin, Germany*
[5]*Max-Planck-Institut für Kernphysik, Saupfercheckweg 1, 69117 Heidelberg, Germany*
[6]*European XFEL, Holzkoppel 4, 22869 Schenefeld, Germany*

(Received 3 February 2025; accepted 26 June 2025; published 15 July 2025)

We report theoretical momentum distributions of electrons ejected from the C and O *K* shells of fixed-in-space CO molecules by Compton scattering of 20 keV photons for different magnitudes and orientations of the photon momentum transfer with respect to the molecular axis. We observe distinct diffraction patterns in our computed momentum distributions, which are governed by the interference of the direct Compton electrons and those which are scattered on the parent and neighboring nuclei. The observed phenomenon is similar to that employed in diffraction imaging using high-energy photoelectrons. It persists after integration over different magnitudes and the orientation of the photon momentum transfer in the molecular frame of reference. A corresponding coincidence experiment confirms our theoretical predictions.

DOI: 10.1103/thh1-8twn

Being a well-established technique in surface science [1], photoelectron diffraction recently attracted an increasing interest in imaging molecular structure and dynamics in the gas phase with tabletop optical lasers [2–4] and free-electron lasers [5–7]. In the latter case, where inner-shell ionization of molecules is addressed, the electron wave employed for the diffraction imaging is initially localized at a well-defined site inside a molecule, and, being multiply scattered by the molecular potential on its way out, it "illuminates the molecule from within" [8]. Detailed information on the target molecule and on the dynamics of a process, accumulated in the photoelectron wave, is uniquely reflected in complex interference patterns observed in the respective angular emission distributions. The most complete information is imprinted in the so-called molecular-frame photoelectron angular distributions (MFPADs, [8–11]). For high-energy photoelectrons, the MFPADs are able to image heavy neighbors and relative positions between atoms. In particular, they exhibit a so-called forward-scattering peak pointing toward the neighboring atom [10,12]. Here, the photoelectron wave emitted in the direction of a heavy neighbor is focused by an uncompensated positive charge of its nucleus, and it may acquire the sense of rotation of the ionizing circularly polarized light [12,13]. In addition, rich double-slit interference petals, which are caused by a superposition of the directly emitted and on-the-neighbor-scattered photoelectron waves, provide information on the distance between the emitter and the scatterer [11,12]. For example, this information imprinted in high-energy MFPADs was recently exploited to follow a molecular breakup on the femtosecond timescale [14].

As the photon energy increases, the cross section for photoionization drops significantly, and, at some point, Compton scattering becomes the dominant light-matter ionization process. Semiclassically, it is treated as a billiard-type collision, in which a photon (as a particle) is deflected and transfers part of its energy and momentum to an electron initially at rest. If this electron is bound in a quantum system, its bound-state momentum distribution needs to be included in the balance [15], which is captured by the so-called impulse approximation (see below). Two recent studies highlighted the need for an even more advanced treatment of the Compton process. Kircher *et al.* [16] found a backward scattering of the Compton electrons

*Contact author: doerner@atom.uni-frankfurt.de
†Contact author: demekhin@physik.uni-kassel.de

and a simultaneous forward kick of the parent nucleus (with respect to the photon momentum transfer $\vec{Q}$). In addition, in a subsequent experimental and theoretical study of Compton ionization of Ne atoms [17], a scattering of the Compton electrons to all angles (being very sensitive to the exact ionic potential) and a Coulomb focusing of the electrons (a reduction of their kinetic energy by the ionization potential) were demonstrated. Since very similar scattering of photoelectron waves on the molecular potential is at the heart of photoelectron diffraction imaging, it was proposed in Ref. [17] that Compton ionization can serve as a potential tool for molecular imaging, as well. Finally, the present Letter provides the still missing proof that Compton electrons enable diffraction imaging of molecules. For this purpose, we theoretically consider the K-shell ionization of carbon and oxygen atoms in CO molecules by Compton scattering of 20 keV photons and report the respective electron momentum distributions.

We recall that, quantum mechanically, the $\hat{A}^2$ part of the light-matter interaction Hamiltonian governs Compton ionization to the lowest order of perturbation theory [18,19]. In particular, the first vector-potential operator annihilates the incoming photon with the initial momentum $\vec{k}_\gamma$ (here, $|\vec{k}_\gamma| = 5.37$ a.u.), and the second one creates the deflected photon with the final momentum $\vec{k}_{\gamma'}$, which corresponds to a photon momentum transfer of $\vec{Q} = \vec{k}_\gamma - \vec{k}_{\gamma'}$. The amplitude for ionization of the initial bound electronic state Ψ_i into the final continuum state $\Psi^-_{\vec{p}}$ with momentum $\vec{p}$ can be computed as [18,19] (atomic units are used throughout)

$$A_{\vec{Q}}(\vec{p}) = \langle \Psi^-_{\vec{p}} | e^{i\vec{Q}\cdot\vec{r}} | \Psi_i \rangle. \quad (1)$$

For high-energy electrons, the final continuum state can be approximated as a plane wave $\Psi^-_{\vec{p}} \approx [1/(2\pi)^{3/2}] e^{i\vec{p}\cdot\vec{r}}$, and the respective amplitude (1) simplifies to

$$A_{\vec{Q}}(\vec{p}) \approx \frac{1}{(2\pi)^{3/2}} \langle e^{i(\vec{p}-\vec{Q})\cdot\vec{r}} | \Psi_i \rangle. \quad (2)$$

As a consequence, the momentum distribution of high-energy Compton electrons is given by the Fourier transform of the initial-state wave function, being additionally displaced by the photon momentum transfer $\vec{Q}$. This simple modeling, known as the above-mentioned impulse approximation, enables us to image wave functions of bound electrons via Compton ionization [20,21]. In order to go beyond the impulse approximation, one needs to employ "real" wave functions for the final continuum states $\Psi^-_{\vec{p}}$ [22] of the molecule, and not just plane waves. Using a partial-wave expansion for $\Psi^-_{\vec{p}}$ [23], the matrix element (1) can be simplified to

$$A_{\vec{Q}}(\vec{p}) = \sum_{\ell m} (-i)^\ell \langle \Psi_{\varepsilon \ell m} | e^{i\vec{Q}\cdot\vec{r}} | \Psi_i \rangle Y_{\ell m}(\theta_p, \phi_p), \quad (3)$$

where $\Psi_{\varepsilon\ell m}$ are the partial electron continuum waves with the kinetic energy $\varepsilon = |\vec{p}|^2/2$, angular momentum ℓ, and its projection on the molecular axis m, and they include respective phase shifts implicitly.

The partial electron continuum waves $\Psi_{\varepsilon\ell m}$ were computed in the present work by the stationary single-center method and code [24,25]. It includes interaction of the active continuum electron with the frozen residual ion by multiple scattering to all orders. The numerical calculations were performed in the Hartree-Fock approximation including partial electron continuum waves with angular momenta up to $\ell \leq 35$ and $|m| \leq 15$, while σ and π orbitals of the electrons bound to the molecule were represented by the single-center expansions with $\ell_b \leq 99$ and $|m_b| \leq 1$ (note that higher projections m are populated if $\vec{Q}$ is perpendicular to the molecular axis). Calculations were performed for different orientation angles β of the photon momentum transfer $\vec{Q}$ with respect to the molecular axis and for its absolute values in the interval $Q_{\min} \leq |\vec{Q}| \leq Q_{\max}$. The maximal value $Q_{\max} = 2|\vec{k}_\gamma| \approx 10$ a.u. corresponds to the backward scattering of the incoming photon, while the minimal value $Q_{\min} = \sqrt{2I_p}$ corresponds to the energy required to overcome the ionization potential I_p ($Q_{\min} \approx 4.7$ a.u. for C 1s and $Q_{\min} \approx 6.4$ a.u. for O 1s). In the numerical calculations of the amplitude (3), the plane wave $e^{i\vec{Q}\cdot\vec{r}}$ was represented by the expansion over spherical harmonics, and the two-dimensional integration over the spatial angles was performed analytically.

Figure 1 depicts two-dimensional slices of the three-dimensional electron momentum distributions, computed for the K-shell ionization of the carbon atom with different values of the photon momentum transfer. The momentum transfer $\vec{Q}$ is oriented along the molecular axis, and both are aligned horizontally along p_z with the carbon atom on the right-hand side (see caption of Fig. 1 for more details on the data representation). For the largest considered value of $|\vec{Q}| = 10$ a.u. (the lower-right panel), the computed momentum distribution exhibits a large spot belonging to direct Compton electrons around $p_z \approx 10$ a.u. This observation is in line with the expectations of the impulse approximation. However, a maximum of the spot (set to 1 in all panels) appears at a somewhat lower value of $p_z <$ 10 a.u. (cf. with magenta circle), and this spot of the direct Compton electrons is not perfectly isotropic with respect to its maximum.

Such a distortion is caused by the Coulomb focusing of the Compton electrons [17], where the energy of a free electron is reduced by the ionization potential. This, in turn, results in a respective reduction of the momentum boost which the electron received being still close to the nucleus.

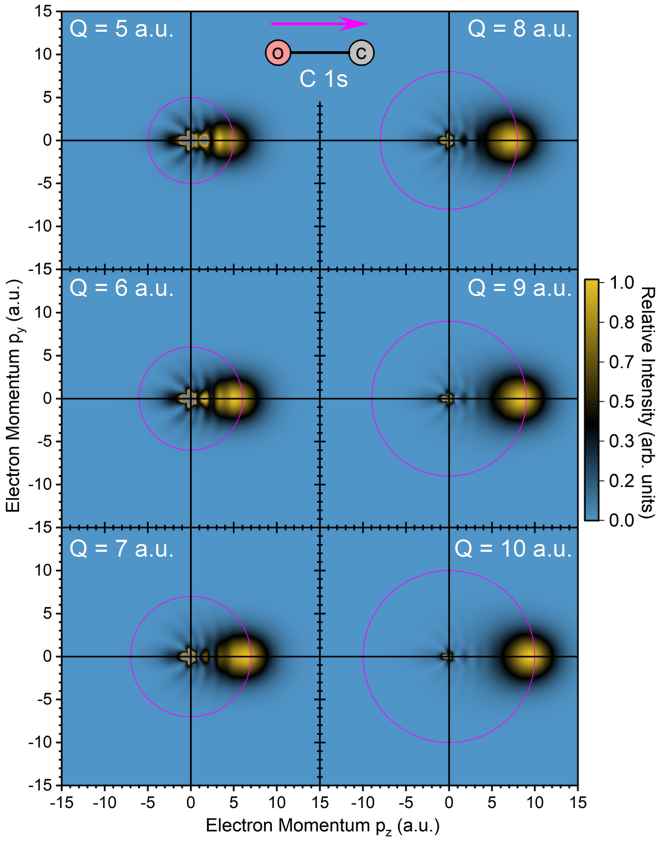

FIG. 1. Molecular-frame momentum distributions of Compton electrons, computed for C 1s ionization of CO and different values of the photon momentum transfer $|\vec{Q}|$ (indicated in each panel and visualized by magenta circles). Shown are slices of the momentum distributions in the $p_z p_y$ plane. The molecule is oriented horizontally along the p_z axis with the carbon atom pointing to the right (see inset on the top panels). The momentum transfer vector $\vec{Q}$ (magenta arrow) is parallel to the molecular axis and points from oxygen to carbon. The distributions are shown on a relative scale normalized to the maximum in the spot of the direct Compton electrons, while the absolute scales of all panels, prior to normalization, differ within 20%.

Another consequence of the focusing effect is the intense spot of low-energy electrons with close-to-zero momenta (note that the respective maximum exceeds the chosen normalization scale). These are electrons with an energy just above the ionization potential (see a model explanation of the focusing effect in Fig. 4 of Ref. [17]). As the value of $|\vec{Q}|$ decreases, the distortions of the distribution of direct Compton electrons and the amount of low-energy electrons, both caused by the focusing effect, increase (see the upper-left panel for the largest effects).

In addition to the known features discussed above, the computed distributions in Fig. 1 illustrate distinct double-slit-type interference patterns, which are more pronounced for the lower values of $|\vec{Q}|$ and even penetrate in the distributions of the direct Compton electrons. These structures are caused by the recently uncovered scattering of the direct Compton electrons to all angles. Contrary to the atoms [16,17], where only a scattering on the parent nucleus can take place, such a scattering of electrons on both, the parent and the neighboring nuclei, is possible in molecules. The effect is enormous, on the order of 30% of the intensity of the direct Compton electrons (see color scale on the right-hand side). Intriguingly, such interference structures can directly be related to the molecular orientation and bond length (see below).

The predicted interference structures appear even more clearly in Fig. 2, where the computed distributions are shown for a fixed value of $|\vec{Q}| = 9$ a.u. and different angles β between the photon momentum transfer and the molecular axis (oriented horizontally). In all cases, the interference patterns build a "wave" on the emitter side of the molecular axis with a planar "wave front," and it is bent toward the scatterer for large values of $|p_y|$. In particular, for the ionization of C 1s electrons (left-hand panels), the wave front is almost planar on the side of the carbon atom ($p_z > 0$), and it is bent strongly on the side of the oxygen ($p_z < 0$). This picture is reversed in the right-hand panels of the figure, where ionization of O 1s electrons is considered. If, for instance, such a distribution is measured in the $\vec{Q}$ frame, and the relative fixed molecular orientation is unknown, it can immediately be deduced from the measured interference patterns.

Figure 3 demonstrates that the observed interference feature is rather robust, and it survives an integration over all considered absolute values and orientations of $\vec{Q}$ in the molecular frame of reference. Here, the integration was performed over the orientation angles $0° \le \beta \le 180°$, such that the photon momentum transfer always points in the upper hemiplane. In addition, contributions of the (anti-) parallel orientations of $\vec{Q}$ are reduced by the solid-angle element. As a consequence, the direct Compton electrons appear on the $p_y > 0$ hemiplane of the distributions, being suppressed along the molecular axis. Such an integration yields the analog to so-called polarization-averaged molecular-frame photoelectron angular distributions [10,11,14], which still preserve information on the molecular geometry and photoionization dynamics [26,27] and result in measured distributions with sufficient statistics.

In total, there are three electron waves, which superimpose: the direct Compton electrons, the direct electrons scattered on the parent nucleus, and those scattered on the neighbor. The first two waves are launched on the same center (the emitter) and, thus, have similar phases (except the scattering phase which varies slowly with the kinetic energy). Therefore, their overlap cannot be responsible for the predicted double-slit-type interference structures, but rather, it shapes a low-energy part of the distributions (gray spots around the origin in Fig. 3). In contrast, the third wave is characterized by the emission-angle-dependent phase, which is proportional to a product of the electron momentum and the distance between the emitter and the

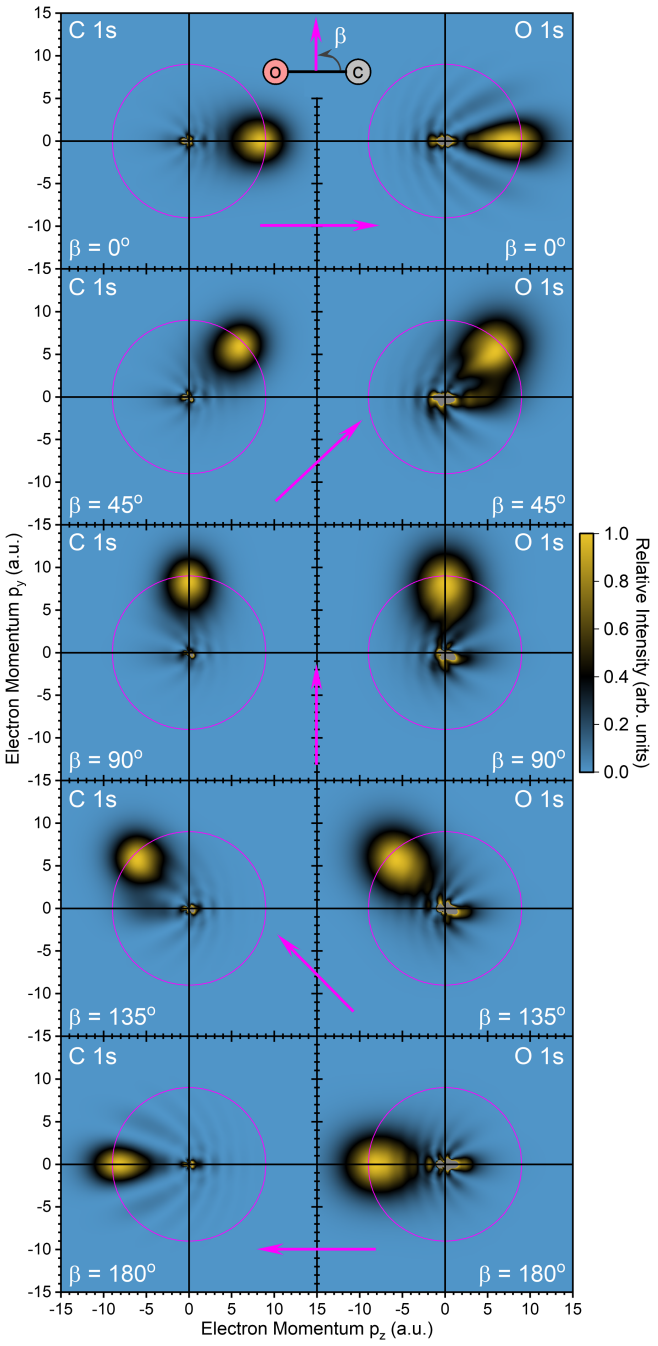

FIG. 2. Molecular-frame momentum distributions of Compton electrons, computed for C 1s (left panels) and O 1s (right panels) ionization of CO by the photon momentum transfer $|\vec{Q}| = 9$ a.u. (indicated by the magenta circles) and different orientation angles β (indicated in each panel) between $\vec{Q}$ and the molecular axis (see sketch on the top panels). Shown are slices of the momentum distributions in the $p_z p_y$ plane, which is given by the molecular axis (along the p_z axis with the carbon atom at the right-hand side) and the photon momentum transfer vector (magenta arrow always points in the upper hemiplane with $p_y > 0$). See the caption of Fig. 1 for more details on the data representation.

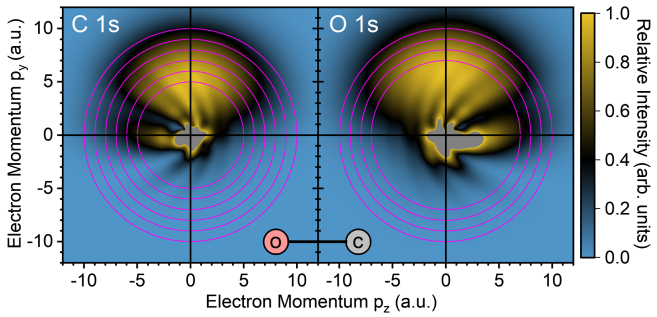

FIG. 3. Molecular-frame momentum distributions of Compton electrons, averaged over all orientations $0° \le \beta \le 180°$ of the photon momentum transfer $\vec{Q}$ (points in the upper hemiplane) with respect to the molecular axis (shown in inset at the bottom) and its absolute values in the intervals of 5 a.u. $\le |\vec{Q}| \le 10$ a.u. for C 1s (left panel) and 7 a.u. $\le |\vec{Q}| \le 10$ a.u. for O 1s (right panel) ionization, as indicated by the magenta circles. See the captions of Figs. 1 and 2 for more details on the data representation.

scatterer [14]. In the upper hemiplane of the momentum distributions ($p_y > 0$) depicted in Fig. 3, the interference is mainly given by the superposition of the dominant direct Compton wave and the weak wave scattered on the neighbor. In the lower hemiplane ($p_y < 0$), where the direct Compton electrons are absent, the two waves scattered on the emitter and on its neighbor superimpose. Since those waves in the lower hemiplane have the same relative phase difference (as the waves superimposing in the upper one) but rather comparable amplitudes, their superposition produces very similar interference patterns but with a higher contrast.

More details can be seen in a polar representation of such averaged distributions, as depicted in the upper panels of Fig. 4. Shown are molecular-frame emission distributions of the Compton electrons from Fig. 3 for particular absolute values of the electron momentum $|\vec{p}|$. The distributions possess a relatively large forward-scattering peak pointing toward the neighboring atom, i.e., toward oxygen or carbon, respectively, in the upper-left or upper-right panels. Moreover, additional interference petals modulate the overall shape of the distributions, and their number grows with increasing electron momentum $|\vec{p}|$ (and it would also grow with an increase of the C–O distance). This picture is fully consistent with a simple analytical model of the double-slit interference between the emitted and scattered photoelectron waves (see Fig. 5 and Eq. (2) in Ref. [14]).

In order to verify these theoretical predictions, we performed an experiment at the beamline ID31 of the European Synchrotron Radiation Facility (ESRF) in Grenoble, France using the cold target recoil ion momentum spectroscopy technique [28,29] (see End Matter for details). The experimental emission distributions of the Compton electrons are compared in the lower panels of

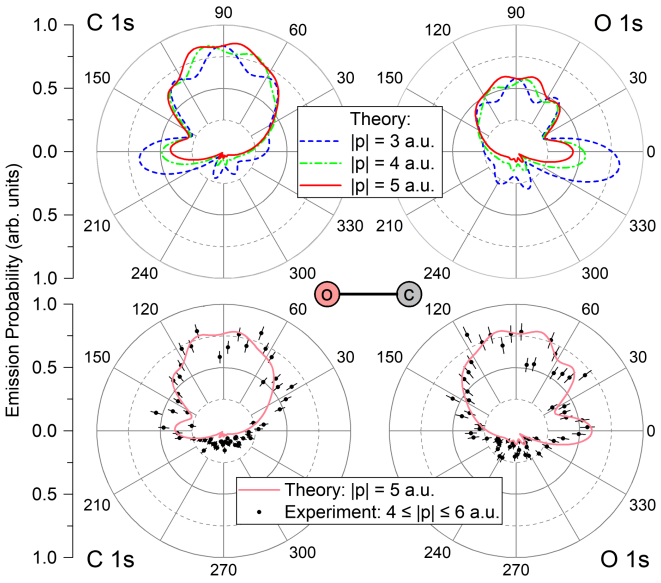

FIG. 4. Polar representation of the averaged emission distributions from Fig. 3 at given absolute values of the electron momentum $|\vec{p}|$ (see legends) for C 1s (left panels) and O 1s (right panels) ionization. Shown are the emission probabilities as functions of the electron emission angle with respect to the molecular axis (oriented horizontally). Curves: theoretical data from Fig. 3. Symbols: experimental data (see text for details). The error bars represent statistical uncertainties. The main lobe pointing toward the neighbor and multiple interference petals are clearly seen in the computed and measured angular distributions.

Fig. 4 with the respective theoretical ones. As in the case of theory, these distributions are averaged over the absolute values and orientations of the photon momentum transfer relative to the molecular axis. In order to gather sufficient statistics, the experimental data represent the interval of 4 a.u. $\leq |\vec{p}| \leq$ 6 a.u. and are additionally integrated over the out-of-plane component of the electron momentum -1.5 a.u. $\leq p_x \leq +1.5$ a.u. (note that the theoretical distributions represent the sharp values of $|\vec{p}|$ and the slices at $p_x = 0$). As one can see from the lower panels of Fig. 4, the experimental distributions agree fairly well with the theoretical ones, supporting the predicted molecular effects, including the main lobe and the multiple interference petals.

In conclusion, we demonstrate, theoretically and experimentally, that ionization by Compton scattering can, indeed, be used for electron diffraction imaging of molecular structure and dynamics. The effect involves scattering of the direct Compton electrons on the nuclei of the ionized atom and its neighbors. The observed double-slit interference patterns in the electron momentum distribution can be directly related to the molecular orientation in space and to the distance between the emitter and the scatterer. Ionization by Compton scattering has an advantage of releasing electrons covering all momenta from zero to approximately $2|\vec{k}_\gamma|$, despite using photons with well-defined energy for their generation. Utilization of free-electron lasers with unprecedented-high flux of hard x-ray photons, especially the new generation of high-repetition-rate x-ray free-electron lasers, may enable ultrafast electron diffraction imaging by this ionization mechanism with sufficient statistics and, thus, resolution. The present findings extend the electron diffraction imaging technique from the low and moderate photon-energy domains (by outer-shell multiphoton ionization with optical photons and inner-shell one-photon ionization with soft x-ray photons) to the hard x-ray domain, where the photoionization mechanism is strongly suppressed.

Acknowledgments—This work was supported by the Deutsche Forschungsgemeinschaft (DFG) and by the Bundesministerium für Bildung und Forschung (BMBF). We acknowledge the European Synchrotron Radiation Facility (ESRF) for provision of synchrotron radiation beamtime under Proposal No. CH-6729 (DOI: 10.15151/ESRF-ES-1299363304) and would like to thank V. Honkimäki, H. Isern, and F. Russello for assistance and support in using beamline ID31. F. T. acknowledges funding by the Deutsche Forschungsgemeinschaft (DFG, German Research Foundation) Project No. 509471550, Emmy Noether Programme. L. K. was supported by DFG Project No. 328961117, SFB 1319 ELCH (Extreme light for sensing and driving molecular chirality). D. M. H., N. M. N., N. D., and P. V. D. acknowledge support by the DFG Project No. 492619011 (DE 2366/6-2).

Data availability—The data that support the findings of this article are openly available at [30], embargo periods may apply.

[1] D. P. Woodruff, Photoelectron diffraction: From phenomenological demonstration to practical tool, Appl. Phys. A **92**, 439 (2008).
[2] M. Meckel, D. Comtois, D. Zeidler, A. Staudte, D. Pavičić, H. C. Bandulet, H. Pépin, J. C. Kieffer, R. Dörner, D. M. Villeneuve, and P. B. Corkum, Laser-induced electron tunneling and diffraction, Science **320**, 1478 (2008).
[3] B. Wolter, M. G. Pullen, M. Baudisch, M. Sclafani, M. Hemmer, A. Senftleben, C. D. Schröter, J. Ullrich, R. Moshammer, and J. Biegert, Strong-field physics with mid-IR fields, Phys. Rev. X **5**, 021034 (2015).
[4] B. Wolter, M. G. Pullen, A.-T. Le, M. Baudisch, K. Doblhoff-Dier, A. Senftleben, M. Hemmer, C. D. Schröter, J. Ullrich, T. Pfeifer, R. Moshammer, S. Gräfe, O. Vendrell, C. D. Lin, and J. Biegert, Ultrafast electron diffraction imaging of bond breaking in di-ionized acetylene, Science **354**, 308 (2016).
[5] F. Krasniqi, B. Najjari, L. Strüder, D. Rolles, A. Voitkiv, and J. Ullrich, Imaging molecules from within: Ultrafast angström-scale structure determination of molecules via photoelectron holography using free-electron lasers, Phys. Rev. A **81**, 033411 (2010).

[6] M. Kazama, T. Fujikawa, N. Kishimoto, T. Mizuno, J. Adachi, and A. Yagishita, Photoelectron diffraction from single oriented molecules: Toward ultrafast structure determination of molecules using x-ray free-electron lasers, Phys. Rev. A **87**, 063417 (2013).
[7] R. Boll *et al.*, Imaging molecular structure through femtosecond photoelectron diffraction on aligned and oriented gas-phase molecules, Faraday Discuss. **171**, 57 (2014).
[8] A. Landers, Th. Weber, I. Ali, A. Cassimi, M. Hattass, O. Jagutzki, A. Nauert, T. Osipov, A. Staudte, M. H. Prior, M. H. Prior, H. Schmidt-Böcking, C. L. Cocke, and R. Dörner, Photoelectron diffraction mapping: Molecules illuminated from within, Phys. Rev. Lett. **87**, 013002 (2001).
[9] T. Jahnke *et al.*, Circular dichroism in K-shell ionization from fixed-in-space CO and N_2 molecules, Phys. Rev. Lett. **88**, 073002 (2002).
[10] J. B. Williams, C. S. Trevisan, M. S. Schöffler, T. Jahnke, I. Bocharova, H. Kim, B. Ulrich, R. Wallauer, F. Sturm, T. N. Rescigno, A. Belkacem, R. Dörner, Th. Weber, C. W. McCurdy, and A. L. Landers, Imaging polyatomic molecules in three dimensions using molecular frame photoelectron angular distributions, Phys. Rev. Lett. **108**, 233002 (2012).
[11] H. Fukuzawa, R. R. Lucchese, X.-J. Liu, K. Sakai, H. Iwayama, K. Nagaya, K. Kreidi, M. S. Schöffler, J. R. Harries, Y. Tamenori, Y. Morishita, I. H. Suzuki, N. Saito, and K. Ueda, Probing molecular bond-length using molecular-frame photoelectron angular distributions, J. Chem. Phys. **150**, 174306 (2019).
[12] I. Vela-Peréz *et al.*, High-energy molecular-frame photoelectron angular distributions: A molecular bond-length ruler, Phys. Chem. Chem. Phys. **25**, 13784 (2023).
[13] H. Daimon, T. Nakatani, S. Imada, S. Suga, Y. Kagoshima, and T. Miyahara, Strong circular dichroism in photoelectron diffraction from nonchiral, nonmagnetic material-direct observation of rotational motion of electrons, Jpn. J. Appl. Phys. **32**, L1480 (1993).
[14] G. Kastirke *et al.*, Photoelectron diffraction imaging of a molecular breakup using an x-ray free-electron laser, Phys. Rev. X **10**, 021052 (2020).
[15] J. W. M. Du Mond, Compton modified line structure and its relation to the electron theory of solid bodies, Phys. Rev. **33**, 643 (1929).
[16] M. Kircher, F. Trinter, S. Grundmann, I. Vela-Perez, S. Brennecke, N. Eicke, J. Rist, S. Eckart, S. Houamer, O. Chuluunbaatar, Y. V. Popov, I. P. Volobuev, K. Bagschik, M. N. Piancastelli, M. Lein, T. Jahnke, M. S. Schöffler, and R. Dörner, Kinematically complete experimental study of Compton scattering at helium atoms near the threshold, Nat. Phys. **16**, 756 (2020).
[17] N. Melzer *et al.*, Role of the Coulomb potential in Compton scattering, Phys. Rev. Lett. **133**, 183002 (2024).
[18] P. M. Bergstrom Jr and R. H. Pratt, An overview of the theories used in Compton scattering calculations, Radiat. Phys. Chem. **50**, 3 (1997).
[19] K. Pisk, Z. Kaliman, and N. Erceg, Wave-particle duality of radiation in Compton scattering, J. Phys. B **49**, 235004 (2016).
[20] M. J. Cooper, P. E. Mijnarends, N. Shiotani, N. Sakai, and A. Bansil, *X-ray Compton Scattering*, Oxford Science Publications Vol. 5 (Oxford University Press, Oxford and New York, 2004).
[21] M. J. Cooper, Compton scattering and electron momentum determination, Rep. Prog. Phys. **48**, 415 (1985).
[22] A. F. Starace, *Theory of Atomic Photoionization*, Handbook of Physics Vol. 31 (Springer, Berlin, 1982).
[23] N. A. Cherepkov, Theory of spin polarisation phenomena in molecular photoionisation processes, J. Phys. B **14**, 2165 (1981).
[24] Ph. V. Demekhin, A. Ehresmann, and V. L. Sukhorukov, Single center method: A computational tool for ionization and electronic excitation studies of molecules, J. Chem. Phys. **134**, 024113 (2011).
[25] N. M. Novikovskiy, A. N. Artemyev, D. V. Rezvan, B. M. Lagutin, and Ph. V. Demekhin, Multichannel single center method, J. Phys. B **55**, 175001 (2022).
[26] F. Ota, K. Yamazaki, D. Sébilleau, K. Ueda, and K. Hatada, Theory of polarization-averaged core-level molecular-frame photoelectron angular distributions: I. A full-potential method and its application to dissociating carbon monoxide dication, J. Phys. B **54**, 024003 (2021).
[27] F. Ota, K. Hatada, D. Sébilleau, K. Ueda, and K. Yamazaki, Theory of polarization-averaged core-level molecular-frame photoelectron angular distributions: II. Extracting the x-ray-induced fragmentation dynamics of carbon monoxide dication from forward and backward intensities, J. Phys. B **54**, 084001 (2021).
[28] R. Dörner, V. Mergel, O. Jagutzki, L. Spielberger, J. Ullrich, R. Moshammer, and H. Schmidt-Böcking, Cold target recoil ion momentum spectroscopy: A 'momentum microscope' to view atomic collision dynamics, Phys. Rep. **330**, 95 (2000).
[29] J. Ullrich, R. Moshammer, A. Dorn, R. Dörner, L. Ph. H. Schmidt, and H. Schmidt-Böcking, Recoil-ion and electron momentum spectroscopy: Reaction-microscopes, Rep. Prog. Phys. **66**, 1463 (2003).
[30] N. Anders, C. Braun, R. Dörner, I. Dwojak, T. Jahnke, L. Kaiser, M. Kircher, J. Kruse, M. A. Kügler, O. D. Mcginnis, N. Melzer, L. Nowak, A. Pier, L. Schmidt, M. Schmidt, L. Sommerlad, J. Stindl, and F. Trinter, Investigating molecular-frame compton electron angular distributions in CO [Dataset], European Synchrotron Radiation Facility, 10.15151/ESRF-ES-1299363304 (2026).
[31] G. B. M. Vaughan, J. P. Wright, A. Bytchkov, M. Rossat, H. Gleyzolle, I. Snigireva, and A. Snigirev, X-ray transfocators: Focusing devices based on compound refractive lenses, J. Synchrotron Radiat. **18**, 125 (2011).
[32] O. Jagutzki, A. Cerezo, A. Czasch, R. Dörner, M. Hattaß, M. Huang, V. Mergel, U. Spillmann, K. Ullmann-Pfleger, T. Weber, H. Schmidt-Böcking, and G. D. W. Smith, Multiple hit readout of a microchannel plate detector with a three-layer delay-line anode, IEEE Trans. Nucl. Sci. **49**, 2477 (2002).
[33] R. Dörner, V. Mergel, L. Spielberger, M. Achler, Kh. Khayyat, T. Vogt, H. Bräuning, O. Jagutzki, T. Weber, J. Ullrich, R. Moshammer, M. Unverzagt, W. Schmitt, H. Khemliche, M. H. Prior, C. L. Cocke, J. Feagin, R. E. Olson, and H. Schmidt-Böcking, Kinematically complete experiments using cold target recoil ion momentum spectroscopy, Nucl. Instrum. Methods Phys. Res., Sect. B **124**, 225 (1997).
[34] J. A. R. Samson, Z. X. He, R. J. Bartlett, and M. Sagurton, Direct measurement of He^+ ions produced by Compton

scattering between 2.5 and 5.5 keV, Phys. Rev. Lett. **72**, 3329 (1994).

[35] L. Spielberger, O. Jagutzki, R. Dörner, J. Ullrich, U. Meyer, V. Mergel, M. Unverzagt, M. Damrau, T. Vogt, I. Ali, Kh. Khayyat, D. Bahr, H. G. Schmidt, R. Frahm, and H. Schmidt-Böcking, Separation of photoabsorption and Compton scattering contributions to He single and double ionization, Phys. Rev. Lett. **74**, 4615 (1995).

[36] M. Schmidt *et al.*, Role of the binding energy on nondipole effects in single-photon ionization, Phys. Rev. Lett. **132**, 233002 (2024).

[37] R. N. Zare, Photoejection dynamics, Mol. Photochem. **4**, 1 (1972), https://web.stanford.edu/group/Zarelab/publinks/zarepub60.pdf.

[38] Th. Weber *et al.*, K-shell photoionization of CO and N_2: Is there a link between the photoelectron angular distribution and the molecular decay dynamics?, J. Phys. B **34**, 3669 (2001).

End Matter

Experimental details—The present experimental setup is very similar to that reported in our previous work [17]. Briefly, a pinhole monochromator [31] was used to select photons from the undulator beam with the energy of 20 keV and a bandwidth of about 2%. A supersonic gas jet of the CO target molecules and the photon beam were crossed at a right angle. The employed parallel 55 V/cm electric and 31 G magnetic fields guided all created electrons and ions, which had an energy below 2 keV, onto two time- and position-sensitive detectors with hexagonal delay-line position readout [32]. In order to accumulate the high-energy Compton electrons emitted to the forward direction, the electron detector with 151 mm active diameter was placed 24 mm off center. To obtain an ion momentum resolution of around 0.7 a.u., the ion arm of the spectrometer with the total length of 840.4 mm was equipped with an electrostatic lens [33]. The Compton events can clearly be separated from the photoionization [34–36], since (for 20 keV photon energy) the latter ions acquire a huge photoelectron recoil momentum of about 37 a.u., while the former are created with momenta below about 11 a.u.

The impact positions on the detectors and measured times-of-flight allow us to reconstruct initial momentum vectors of the detected charged particles. Only events with two electrons and two ions detected in coincidence were considered in the analysis. The electron-energy distributions show clear peaks at the energies of around 255 and 500 eV corresponding to C 1s and O 1s Auger electrons. This was used to distinguish events where the second electron (considered to be the Compton electron) was emitted from the C or the O K shell. The photon momentum transfer vector $\vec{Q}$ was deduced by exploiting momentum conservation for each event. After the K-shell-ionized molecule undergoes an ultrafast Auger decay, the created dication fragments by the Coulomb explosion. We selected events where the kinetic energy release was larger than 10 eV. Only, in this case, the axial recoil approximation [37] is known to be valid [38], and the difference of the momenta of the two ions represents an orientation of the molecular axis with respect to $\vec{Q}$ at the instant of ionization, while the momentum of the Compton electron yields its emission angle with respect to the deduced molecular axis.